Structural Basis of Multivalent Binding to Wheat Germ Agglutinin

David Schwefel,[†] Caroline Maierhofer,[‡] Johannes G. Beck,[‡] Sonja Seeberger,[‡] Kay Diederichs,[†] Heiko M. Möller,[‡] Wolfram Welte,*[†] and Valentin Wittmann*[‡]*

[‡] Department of Chemistry, [†] Department of Biology, Universität Konstanz, Universitätsstr. 10, 78457 Konstanz, Germany

Supporting Information

Contents

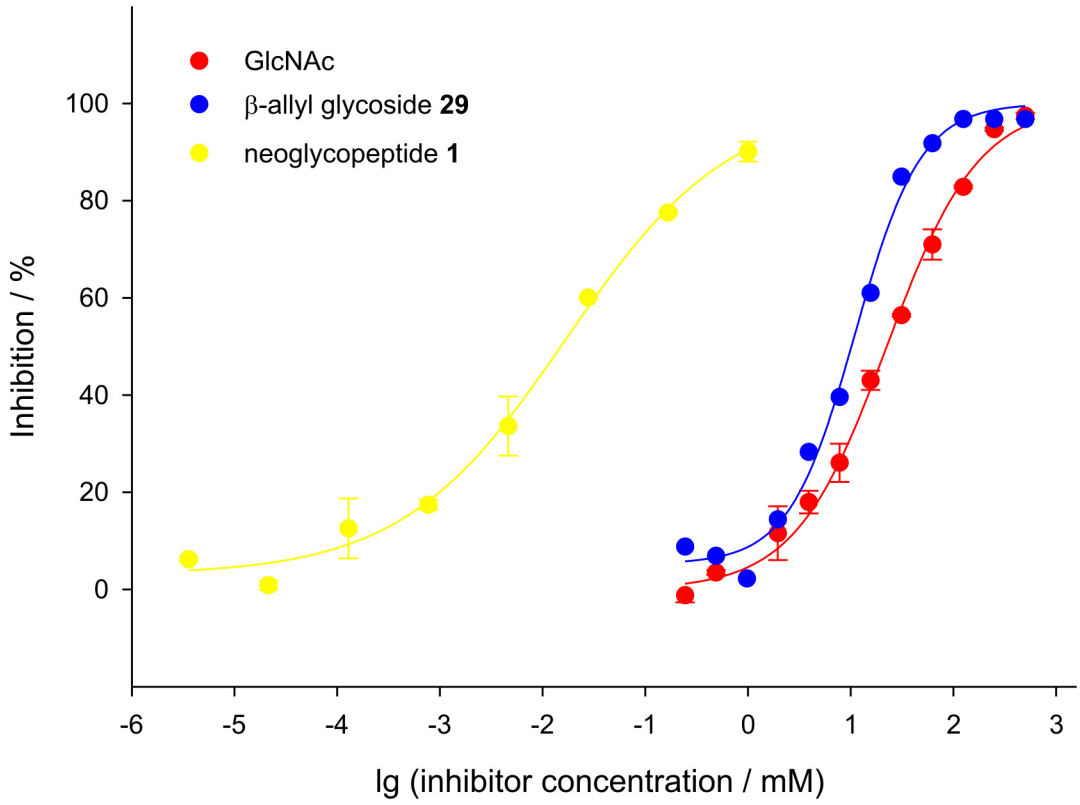

Figure S1. Dose-response curves for inhibition of binding of horseradish peroxidase-labeled WGA to β-GlcNAc-modified microtiter plates by GlcNAc, **1**, and **29**.

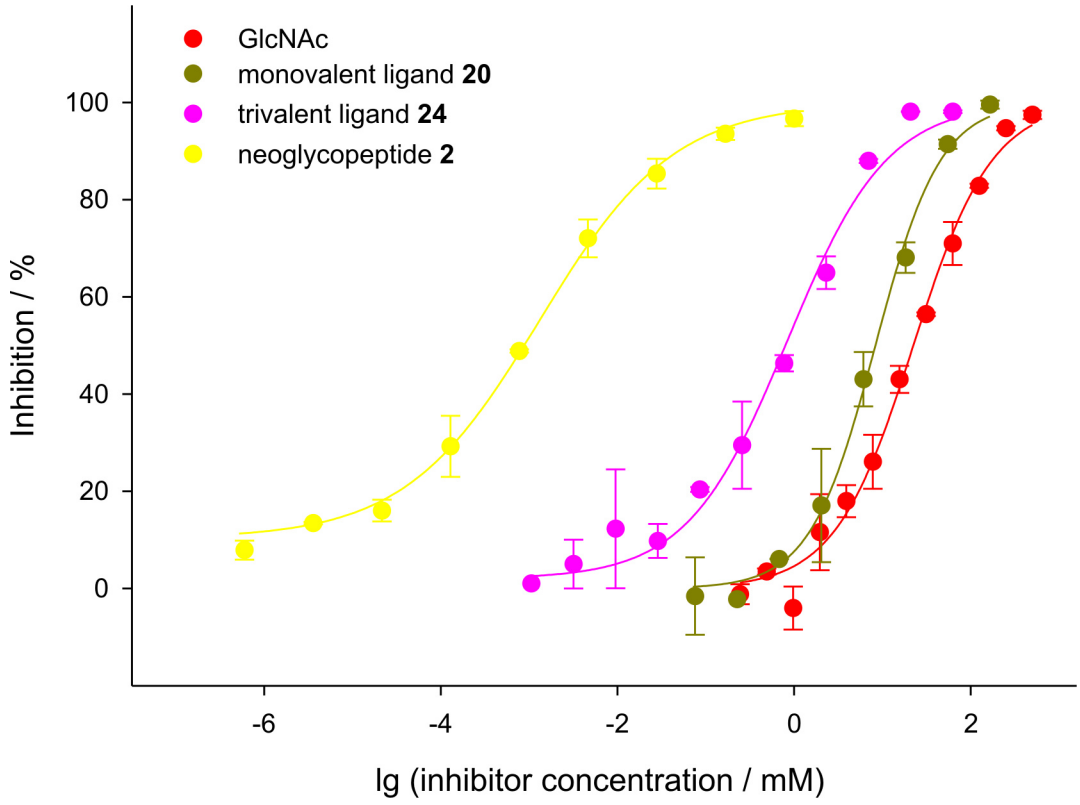

Figure S2. Dose-response curves for inhibition of binding of horseradish peroxidase-labeled WGA to β-GlcNAc-modified microtiter plates by GlcNAc, **2**, **20**, and **24**.

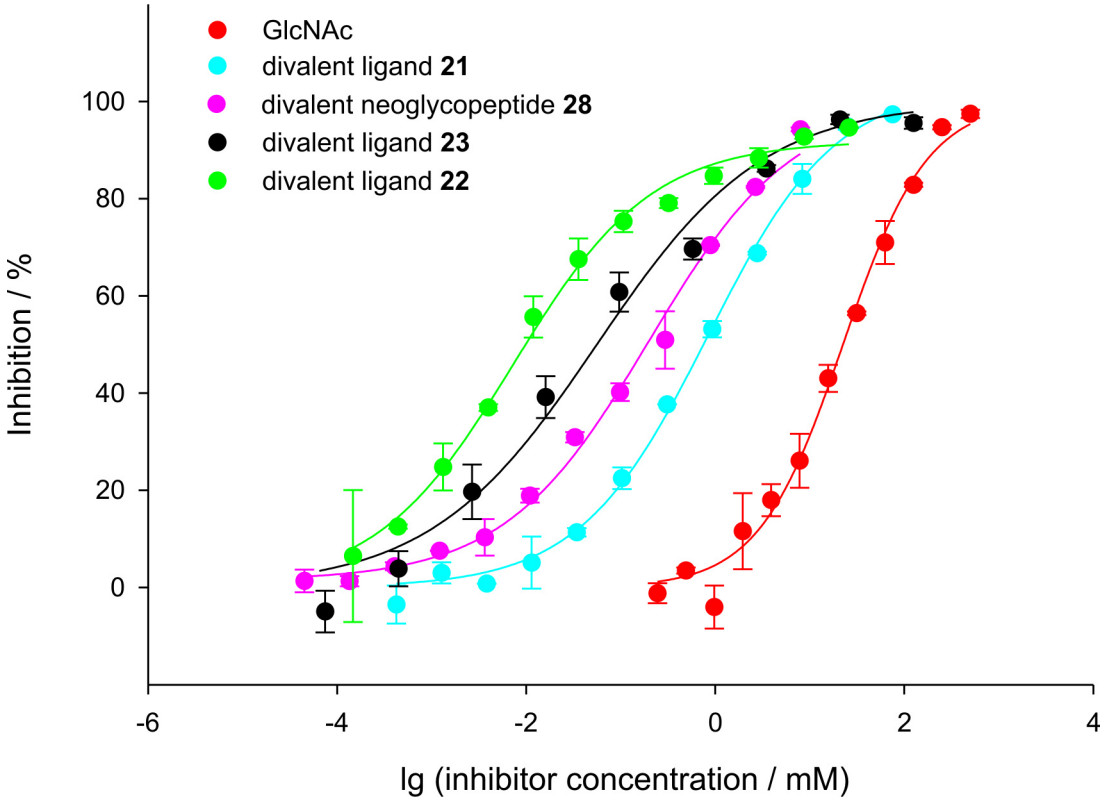

Figure S3. Dose-response curves for inhibition of binding of horseradish peroxidase-labeled WGA to β-GlcNAc-modified microtiter plates by GlcNAc, **21**, **22**, **23**, and **28**.

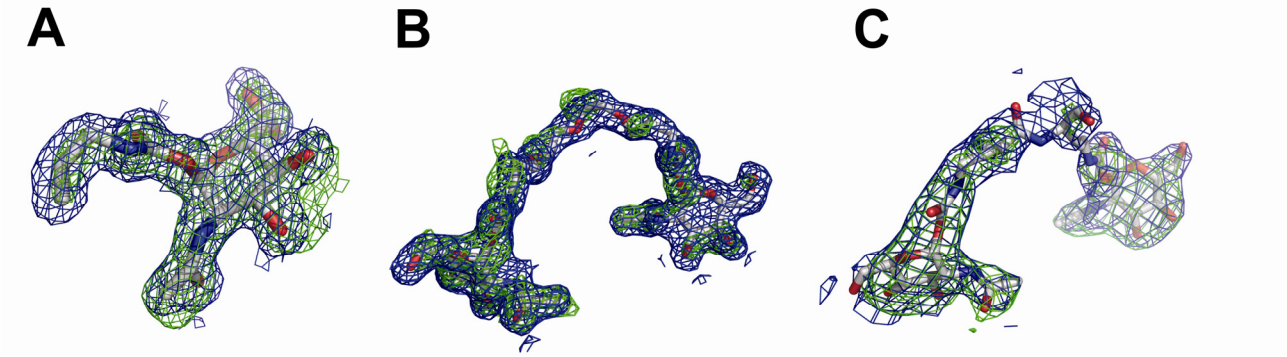

Figure S4. Unbiased F_o–F_c (green, contoured at 2.5σ) and refined 2 F_o–F_c (blue, contoured at 1σ) electron densities for (A) propyl carbamate **20** at binding site B1C2, (B) divalent ligand **23** at the binding site pair B1C2 – C2B1, and (C) visible substructure of cyclic peptide **2** at the binding site pair B1C2 – C2B1 The refined atomic models of the respective compounds are shown in stick representation with carbon atoms colored white, nitrogens blue and oxygens red.

Table S1. ^{1}H and ^{13}C NMR chemical shifts (ppm) of neoglycopeptide **2** in H_2O/D_2O (95:5, pH 5) at 300 K. ^{1}H and ^{13}C Chemical shifts were referenced to 3-(trimethylsilyl)-2,2,3,3-tetradeuteropropionic acid (TSP). n.d., not determined

	H^N	H^α	C^α	H^β	C^β	H^γ	C^γ	others
Lys-1	6.987	3.971	55.75	1.722	30.98	1.332 / 1.390	22.45	H^δ/C^δ: 1.526 / 28.20; $H^\varepsilon/C^\varepsilon$ 3.189 / 39.24; H^ζ: 7.886
D-Dab-2	8.499	4.320	52.24	1.938 / 2.093	29.93	3.132 / 3.265	37.15-37.30	H^δ: 7.274
D-Val-3	7.812	4.123	59.57	2.085		0.922	17.76 / 18.52	
D-Dab-4	8.322	4.398	51.84	1.93 / 2.054	30.70	3.216	37.15-37.30	H^δ: 7.255
D-Dab-5	8.283	4.499	50.91	1.874 / 2.073	30.88	3.164 / 3.236	37.15-37.30	H^δ: 7.222
D-Val-6	8.131	4.010	60.96	2.127	27.23	0.975	18.50	
D-Dab-7	8.594	4.240	52.18	1.988 / 2.111		3.234	37.15-37.30	H^δ: 7.256
Glu-8	7.911	4.177	53.98	2.006 / 2.093		2.287 / 2.356	32.07	
β-Ala-9	8.051	3.404 / 3.503	34.55	2.490	35.86			$CONH_2$: 6.863 / 7.534

	H-1 / C-1	H-2 / C-2	H-3 / C-3	H-4 / C-4	H-5 / C-5	H-6 / C-6	H^N	H^{Me} / C^{Me}
GlcNAc	5.91-5.94 / 91.6	4.03-4.06 / 52.6	3.77 / 70.7	3.57-3.60 / 69.4	3.72 / 73.7	3.80 / 60.3	8.26-8.29	2.020-2.032 / 21.8

	H^{tBu}	C^{Me}	C^{quart}
Boc	1.427	27.47	n.d.

Table S2. Structure determination of neoglycopeptide **2** in solution. Internuclear distances as determined from NOESY cross peak integrals were used as upper distance bounds during molecular dynamics simulated annealing within AMBER 8.

Atom 1	Atom 2	Distance [Å]
D-Dab-4/5/7-$H^{\gamma 1/2}$	D-Val-3 $H^{\gamma 1/2}$	4,85
D-Dab-4/5/7-$H^{\gamma 1/2}$	D-Val-6 $H^{\gamma 1/2}$	4,54
Lys-1 H^{α}	D-Dab-2 H^{N}	2,93
Lys-1 H^{N}	D-Dab-2 H^{N}	3,72
Lys-1 $H^{\beta 1/2}$	D-Dab-2 H^{N}	4,40
Lys-1 H^{ζ}	D-Val-3 $H^{\gamma 1/2}$	4,80
D-Dab-2 H^{N}	Lys-1 $H^{\gamma 1}$	4,28
D-Dab-2 H^{N}	Lys-1 $H^{\gamma 2}$	4,28
D-Dab-2 H^{N}	D-Val-3 H^{N}	3,30
D-Dab-2 H^{α}	D-Val-3 H^{N}	4,16
D-Val-3 H^{N}	D-Dab-2/4-$H^{\beta 1/2}$	3,98
D-Dab-4 H^{N}	D-Val-3 H^{N}	4,09
D-Dab-4 H^{N}	D-Val-3 $H^{\gamma 1/2}$	4,32
D-Dab-4 H^{α}	D-Dab-5 H^{N}	3,24
D-Dab-5 H^{α}	D-Val-6 H^{N}	3,66
D-Dab-5 $H^{\beta 1/2}$	D-Val-6 H^{N}	4,16
D-Val-6 H^{N}	D-Dab-4/5/7-$H^{\gamma 1/2}$	4,64
D-Val-6 H^{α}	D-Dab-7 H^{N}	2,88
D-Dab-7 H^{N}	D-Val-6 $H^{\gamma 1/2}$	4,40
D-Dab-7 H^{N}	D-Val-6 H^{N}	3,60
D-Dab-7 H^{N}	Glu-8 H^{N}	3,54
D-Dab-7 H^{α}	Glu-8 H^{N}	3,48
Glu-8 $H^{\gamma 1}$	Lys-1 H^{ζ}	3,18
Glu-8 $H^{\gamma 2}$	Lys-1 H^{ζ}	3,18
Glu-8 H^{N}	D-Val-6 H^{α}	4,38
Glu-8 H^{N}	D-Val-6 $H^{\gamma 1/2}$	4,70
Glu-8 H^{α}	β-Ala-9 H^{N}	3,25
β-Ala-9 H^{N}	D-Val-6 $H^{\gamma 1/2}$	4,65
β-Ala-9 H	Glu-8 $H^{\beta 1/2}$	3,83

Table S3. Structure determination of neoglycopeptide **2** in solution. $^3J_{HNH\alpha}$ coupling constants as determined from DQF-COSY spectra were employed during molecular dynamics simulated annealing within AMBER 8 as direct *J*-coupling restraints with the following Karplus parameters: $^3J_{HH} = A \cos^2\phi + B \cos\phi + C$, parameters: $A = 7.9$, $B = -1.55$, $C = 1.35$

Residue	D-Val-3	D-Dab-4	D-Dab-5	D-Dab-7
$^3J_{HNH\alpha}$ [Hz]	8.4	8.8	8.8	8.1

Table S4. Structure determination of neoglycopeptide **2** in solution. $^3J_{H\alpha H\beta}$ coupling constants as determined from DQF-COSY spectra indicate that the χ1 dihedral angles of D-Dab residues 2, 4, 5, and 7 do not adopt g^- rotamers and Glu-8 does not adopt the g^+ rotamer. These rotamers were excluded by χ1 torsion angle restraints during molecular dynamics simulated annealing within AMBER 8.

Residue	D-Dab-2	D-Dab-4	D-Dab-5	D-Dab-7	Glu-8
$^3J_{H\alpha H\beta}$ [Hz]	12	12	10	11	10
$^3J_{H\alpha H\beta'}$ [Hz]	6	6	5	6	5
allowed χ1	120 ± 120	120 ± 120	120 ± 120	120 ± 120	–120 ± 120

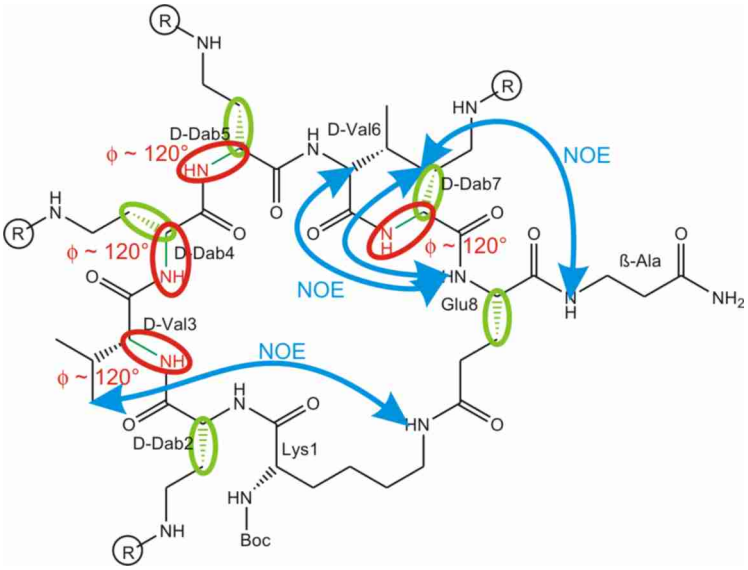

Figure S5. Structure determination of neoglycopeptide **2** in solution. Long-range (i.e. non-sequential) distance constraints are shown as blue arrows. φ dihedral angles restrained by direct *J*-coupling restraints are marked with red circles. χ1 Dihedral angle restraints are marked with green circles.

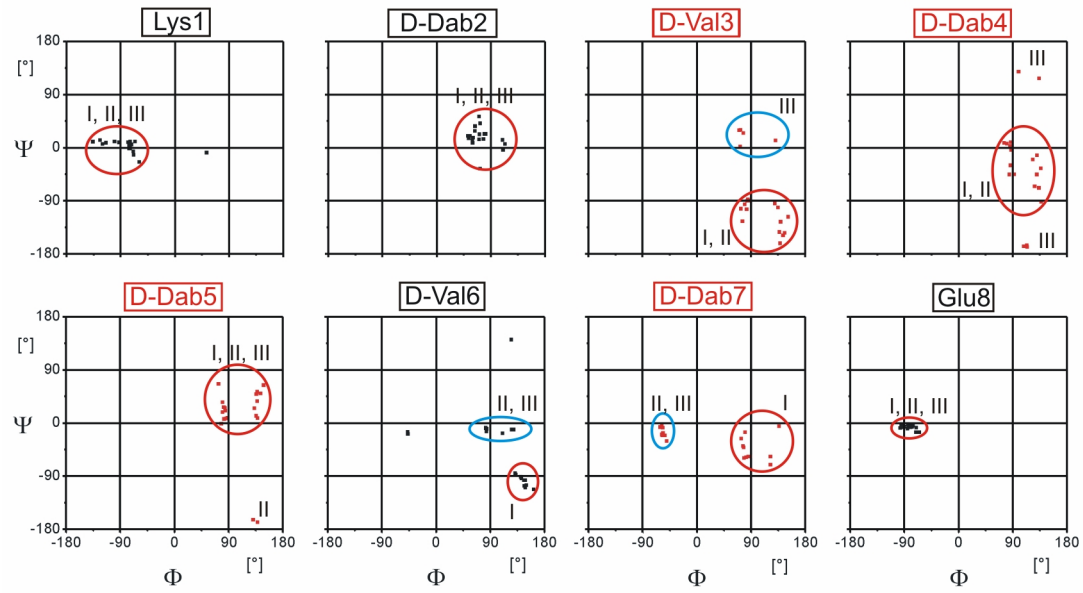

Figure S6. Structure determination of neoglycopeptide **2** in solution. Ramachandran plot of the final ensemble of 20 conformers. The conformers can be grouped into three families of conformers, I, II, and III, according to backbone rmsd after superposition.

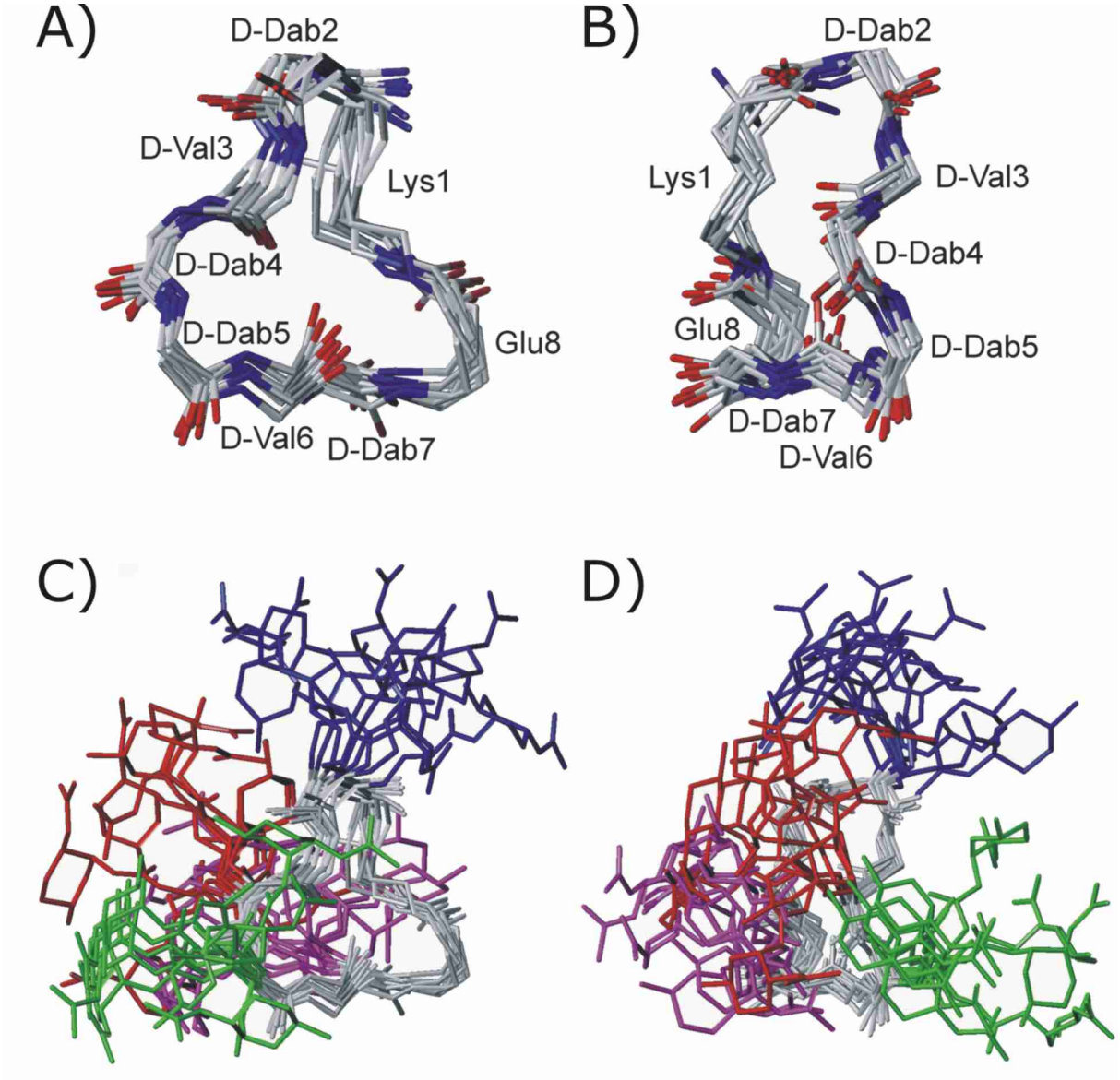

Figure S7. Structure determination of neoglycopeptide **2** in solution: Ensemble of the dominant family of conformers of **2**. (A) Peptide backbone structures, (B) ensemble turned by 90° around the vertical axis. (C) Orientations of sugar-bearing side chains, (D) ensemble turned by 90° around the vertical axis (blue D-Dab-2, red D-Dab-4, green D-Dab-5, magenta D-Dab-7).

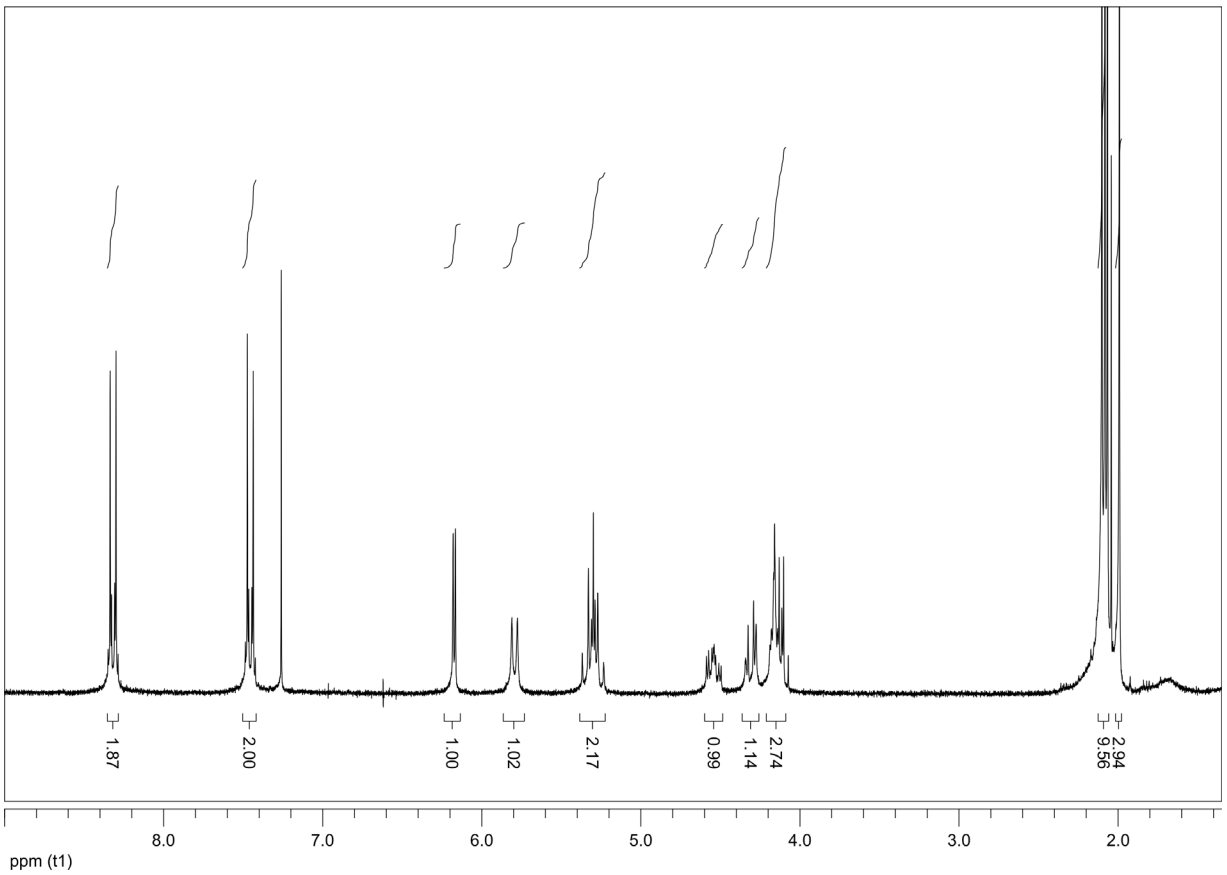

^{1}H NMR of **5** ($CDCl_3$, 250.1 MHz)

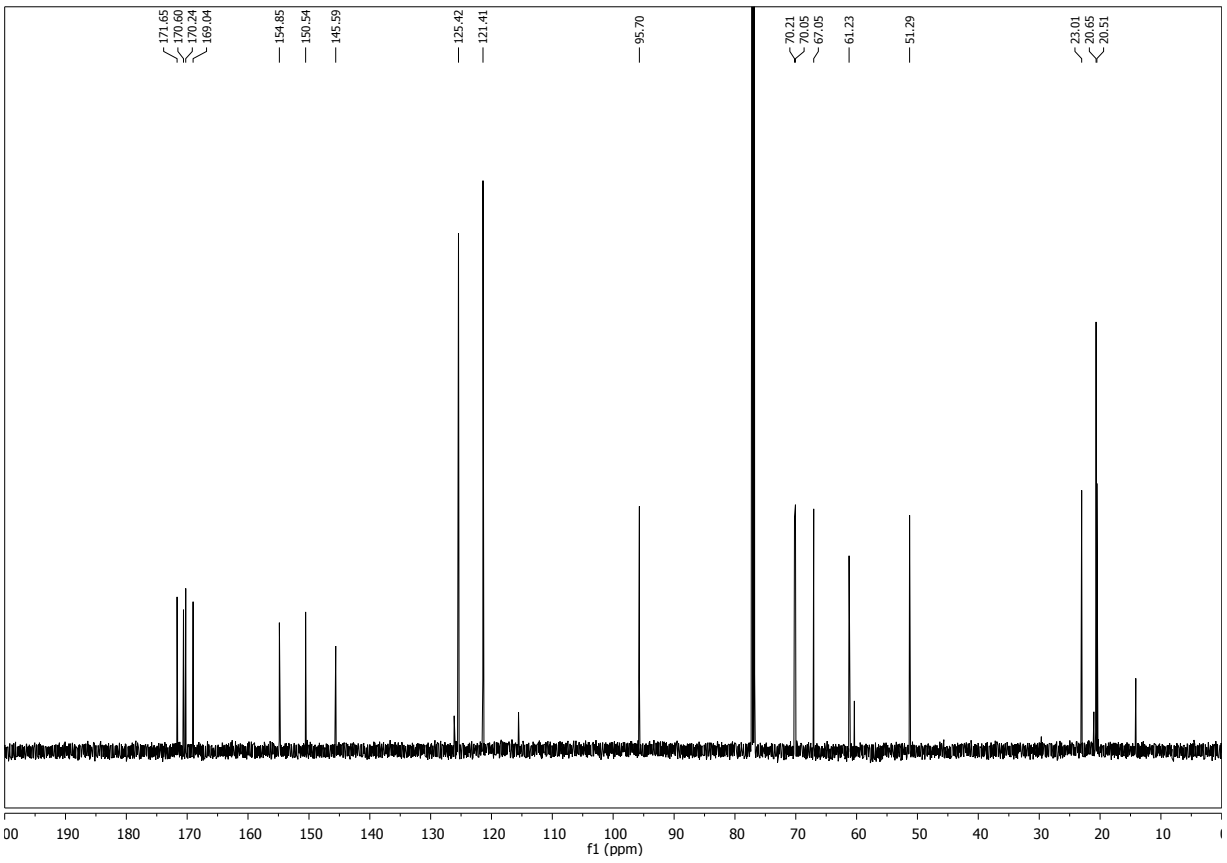

^{13}C NMR of **5** ($CDCl_3$, 150.9 MHz)

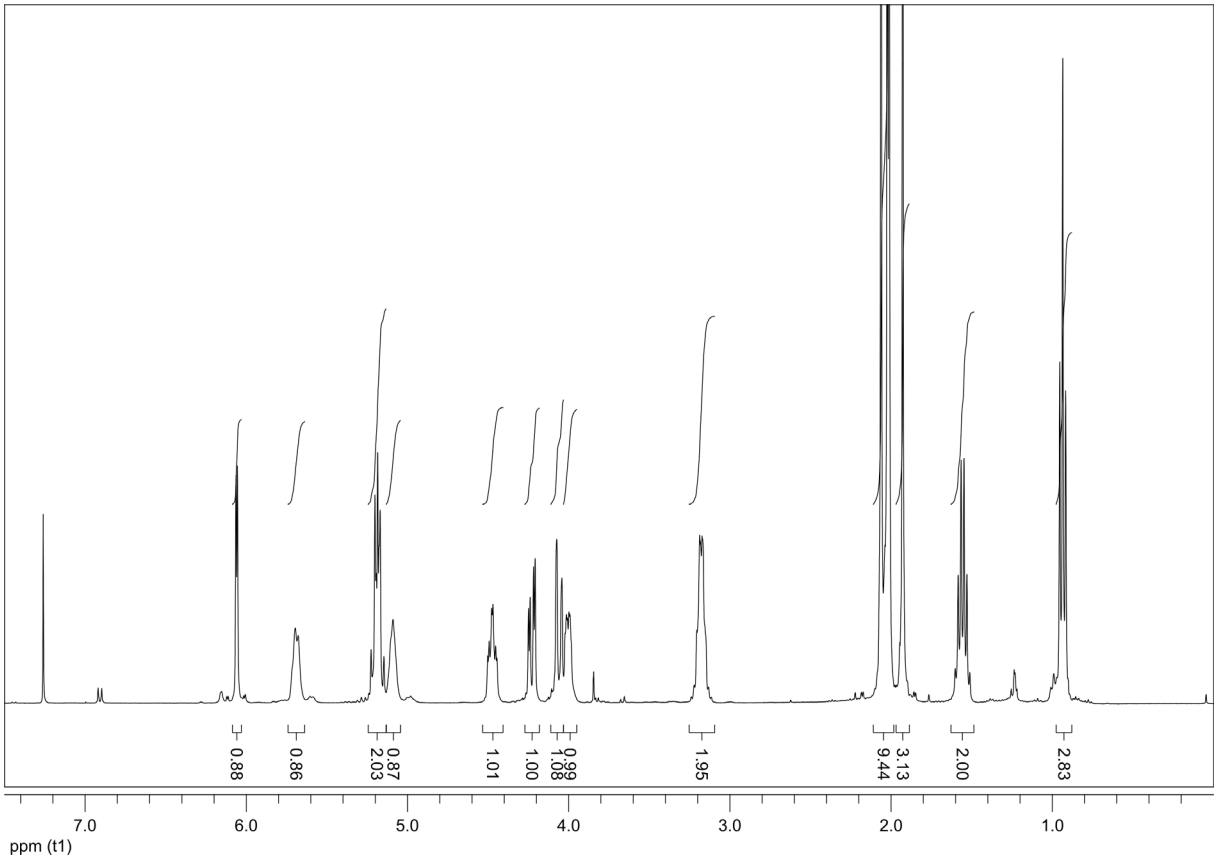

^{1}H NMR of **15** ($CDCl_3$, 400.1 MHz)*

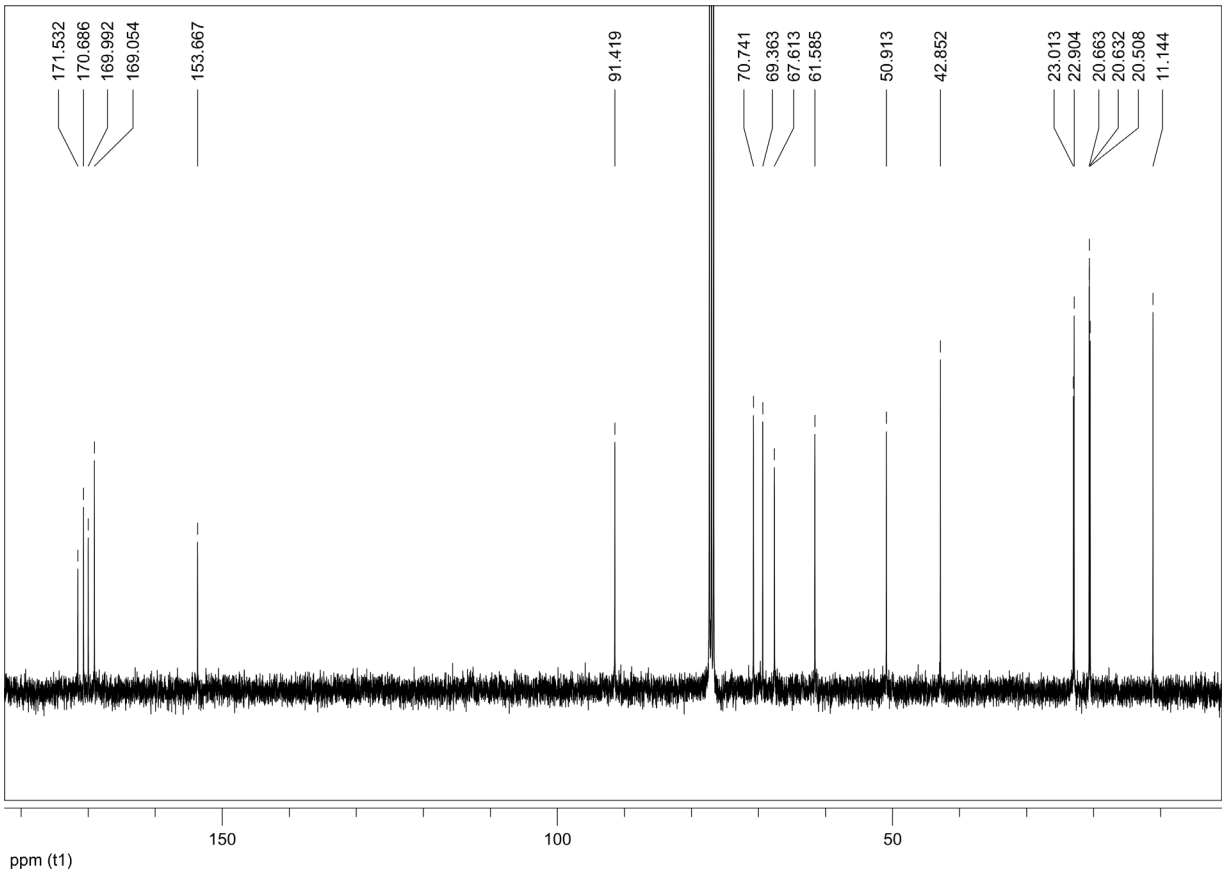

^{13}C NMR of **15** ($CDCl_3$, 100.6 MHz)

* The set of signals with lower intensity originates from a minor isomer due to *cis*-*trans* isomerization of the carbamate moiety, as was shown by observation of corresponding exchange signals in ROESY spectra.

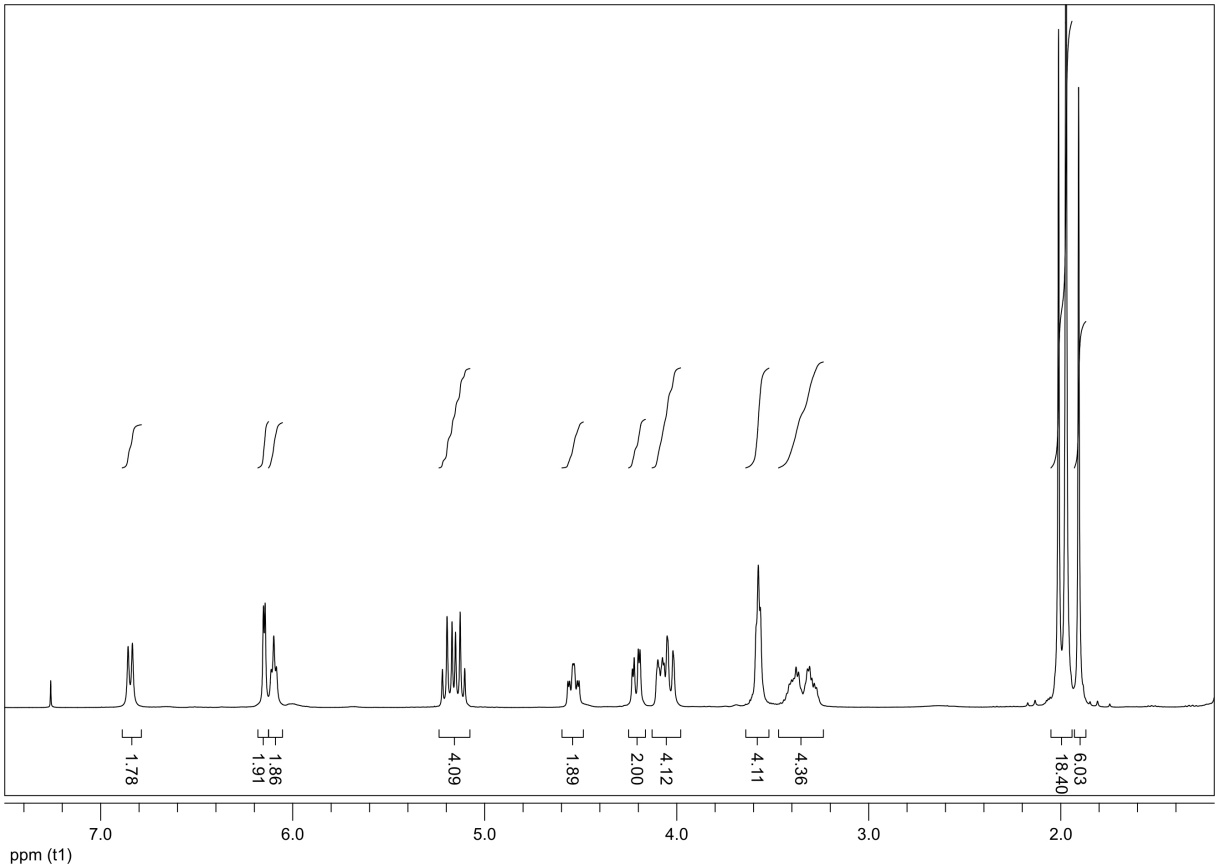

^{1}H NMR of **16** ($CDCl_3$, 400.1 MHz)

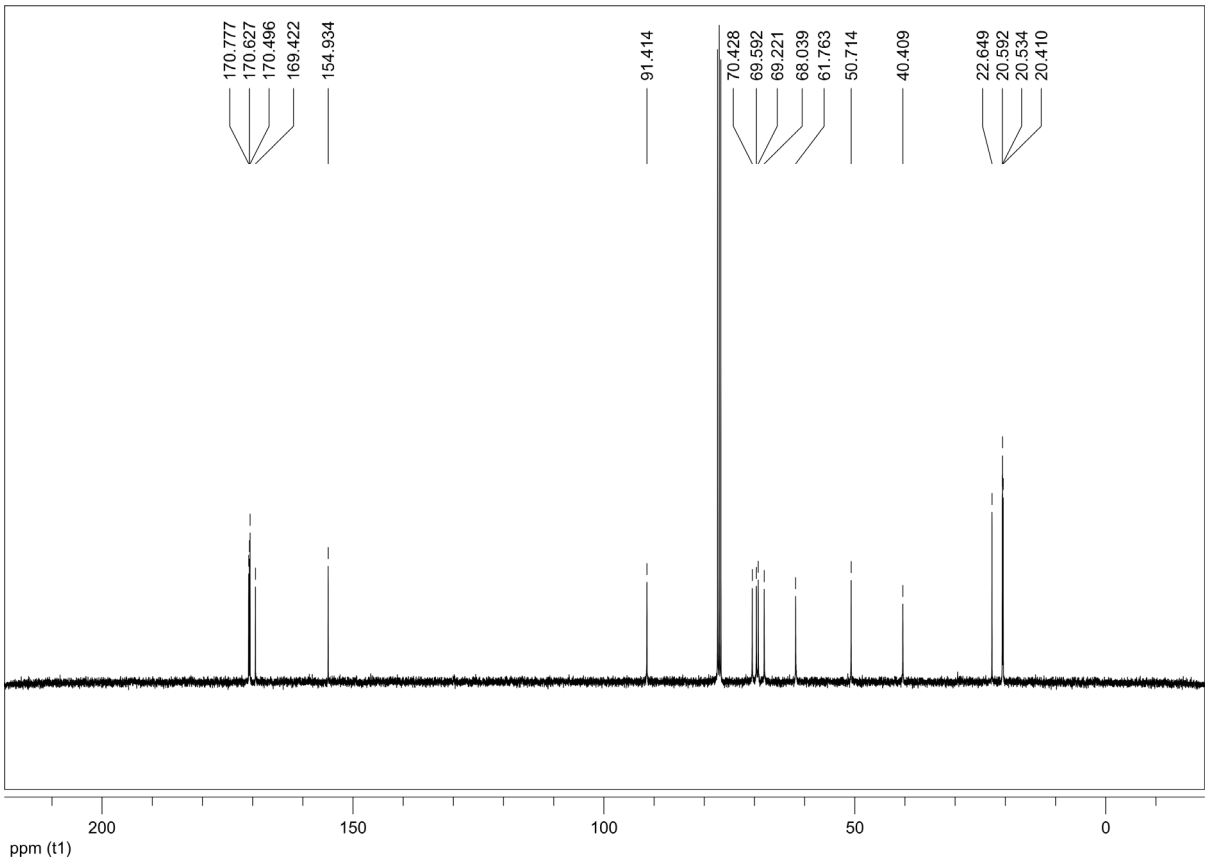

^{13}C NMR of **16** ($CDCl_3$, 100.6 MHz)

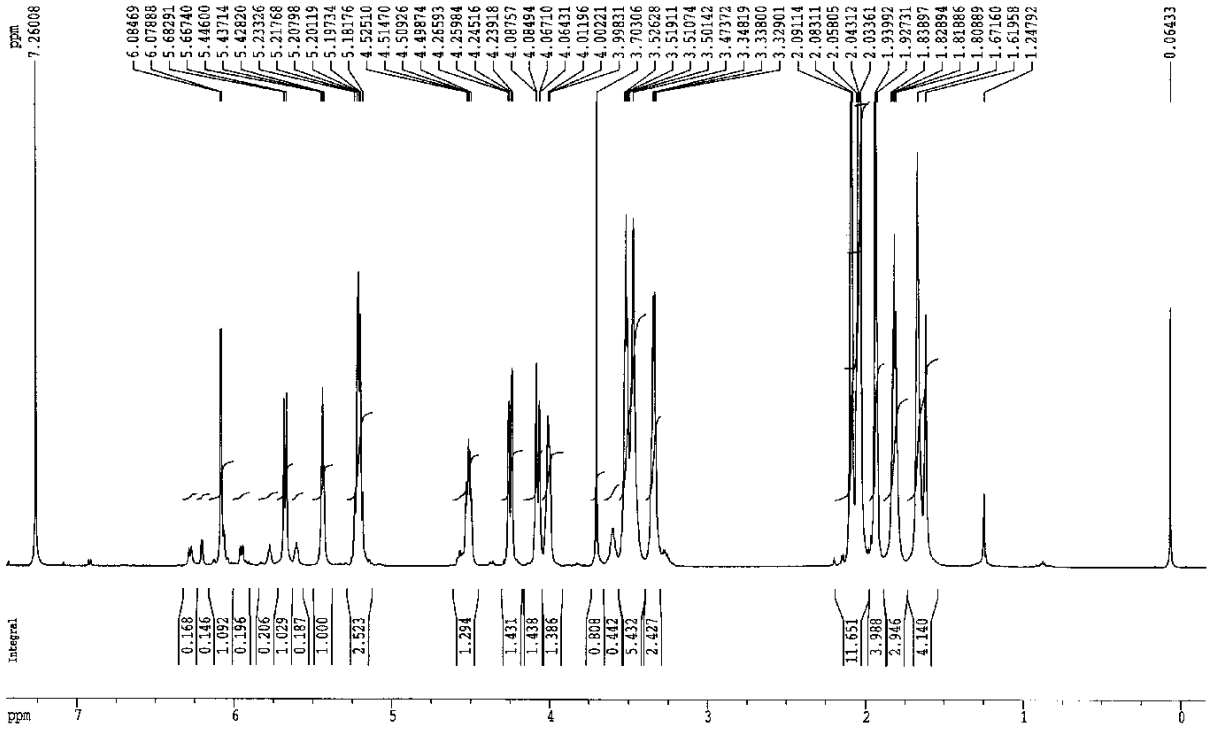

^{1}H NMR of **17** ($CDCl_3$, 600.1 MHz)*

* The set of signals with lower intensity originates from minor isomers due to *cis-trans* isomerization of the carbamate moieties, as was shown by observation of corresponding exchange signals in ROESY spectra (cf. below).

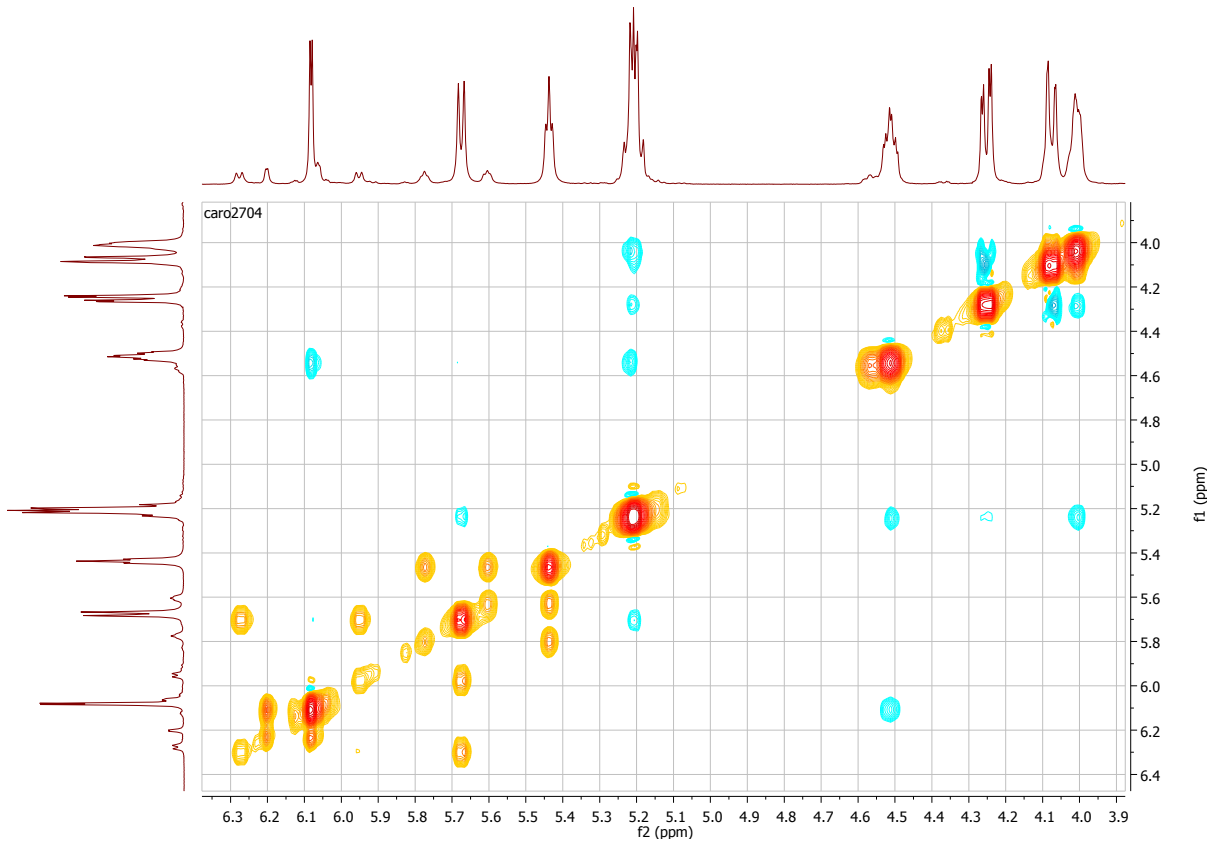

ROESY NMR of **17** ($CDCl_3$, 600.1 MHz). Orange cross peaks (with the same sign as the diagonal) indicate chemical exchange whereas cyan cross peaks originate from dipolar cross relaxation (spatial vicinity).

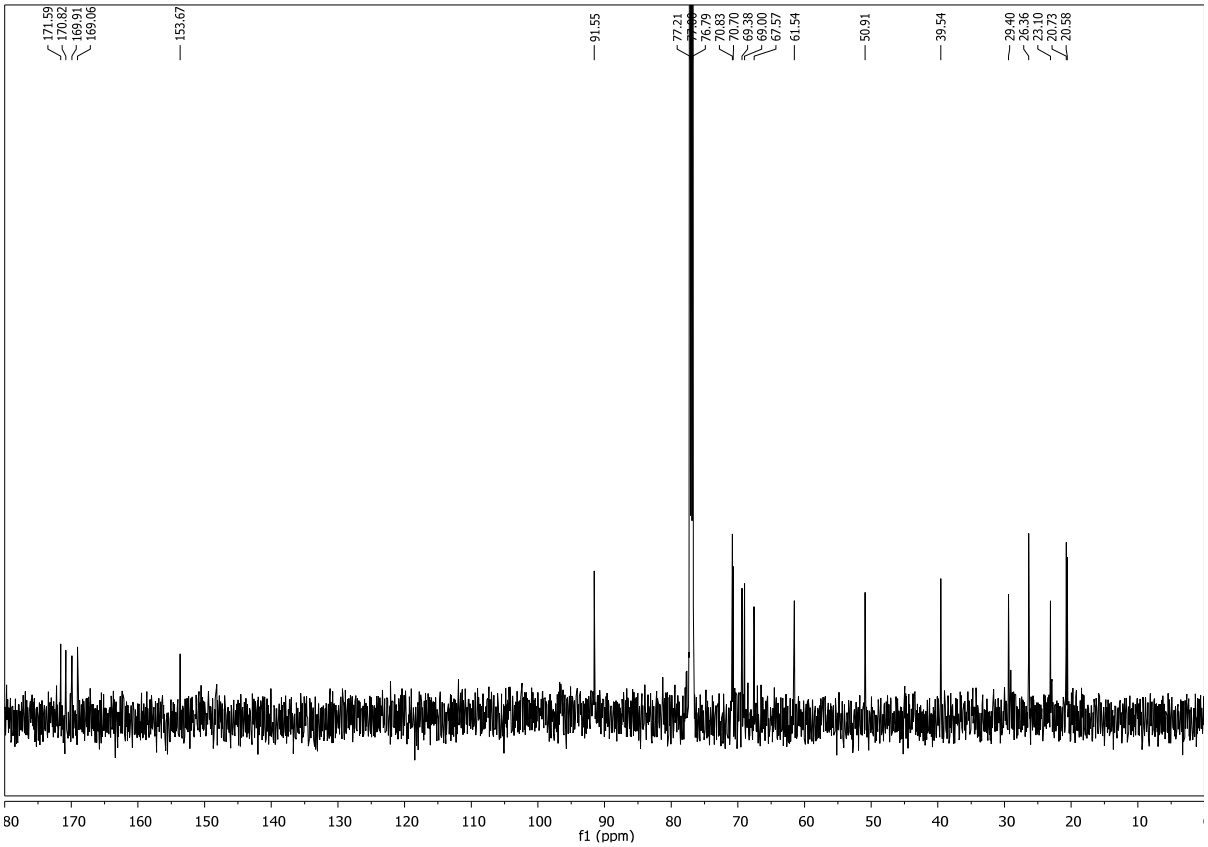

^{13}C NMR of **17** ($CDCl_3$, 150.9 MHz)

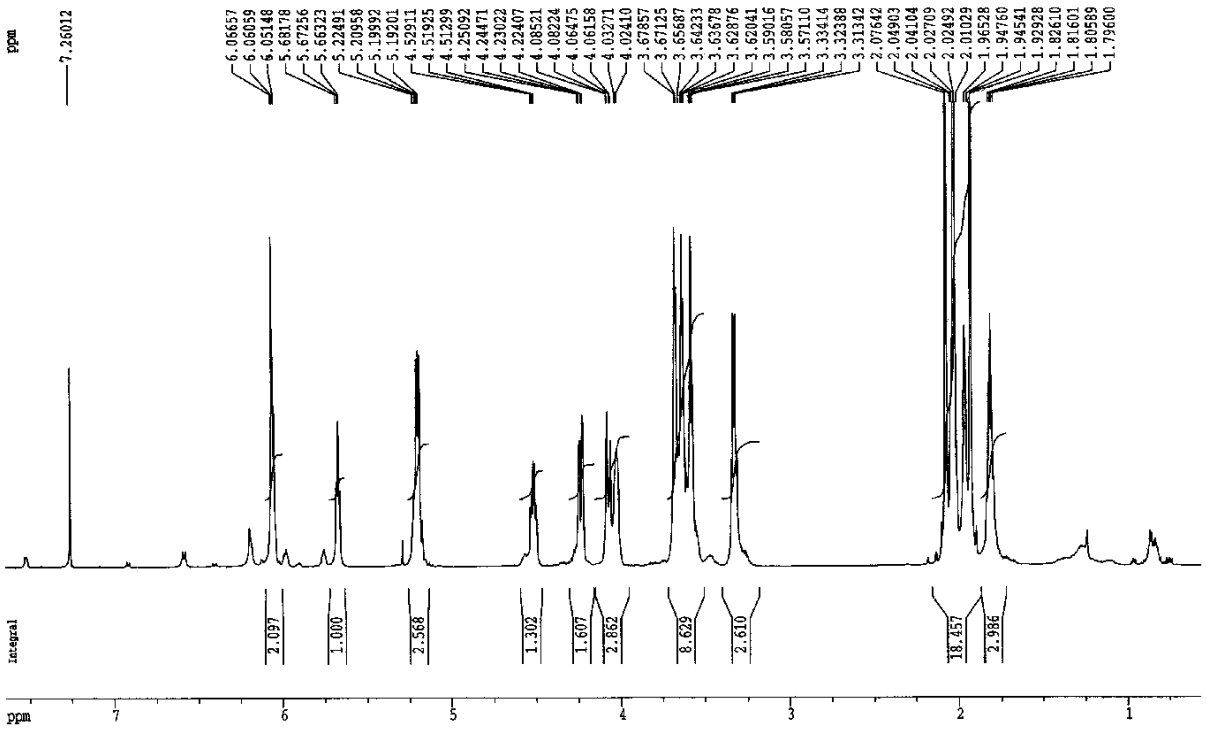

^{1}H NMR of **18** ($CDCl_3$, 600.1 MHz)*

* The set of signals with lower intensity originates from minor isomers due to *cis-trans* isomerization of the carbamate moieties, as was shown by observation of corresponding exchange signals in ROESY spectra.

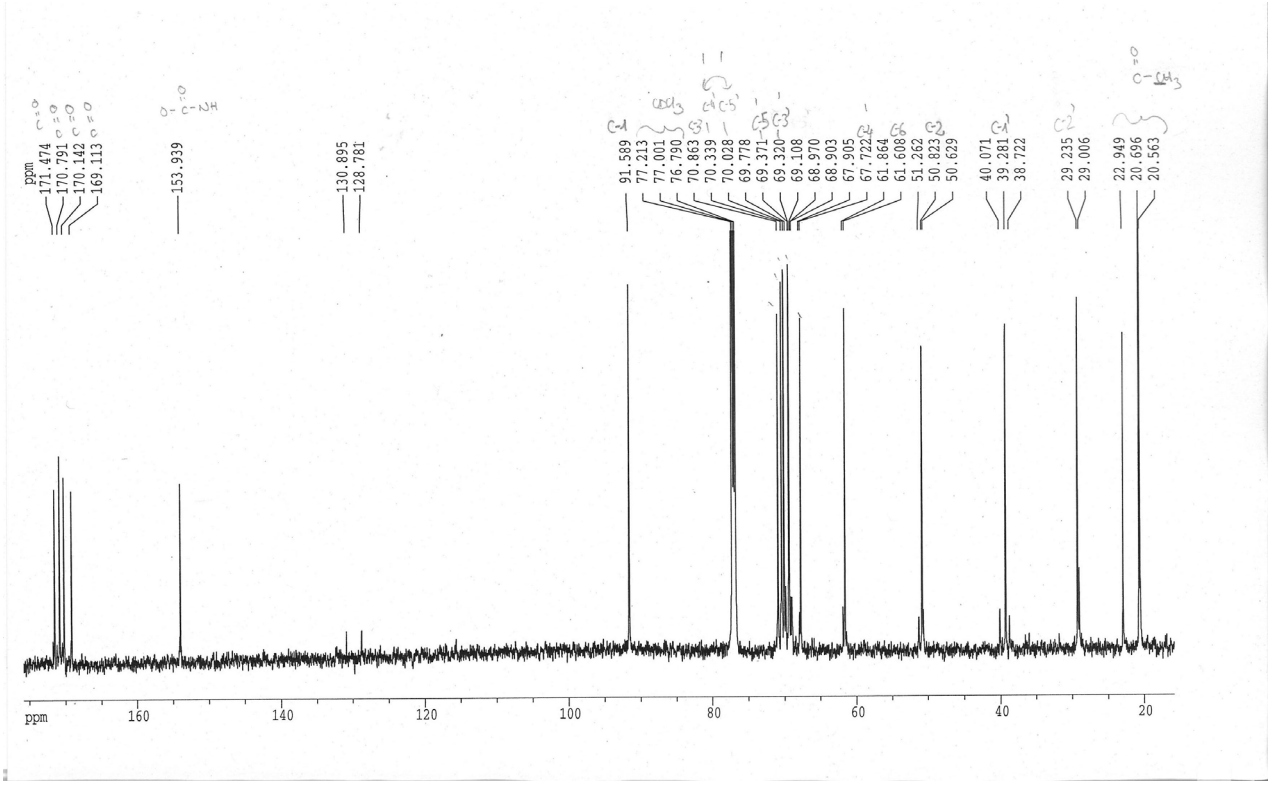

^{13}C NMR of **18** ($CDCl_3$, 150.9 MHz)

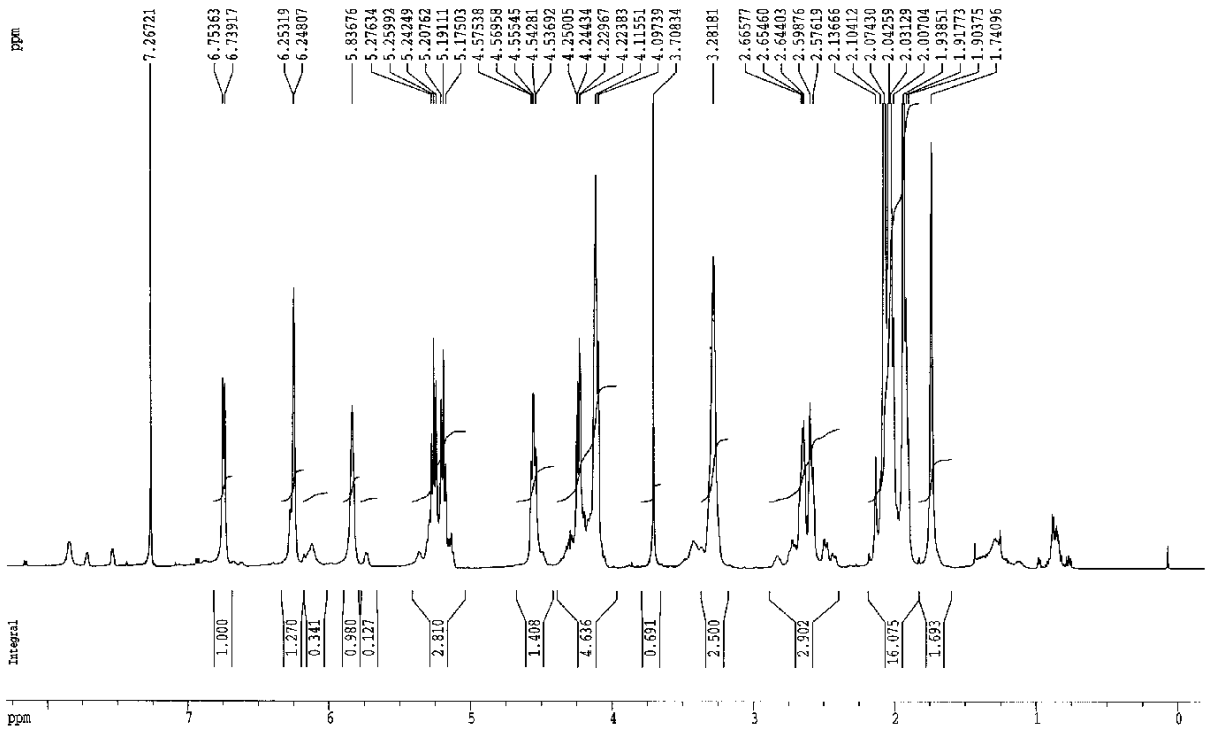

^{1}H NMR of **19** ($CDCl_3$, 600.1 MHz)*

* The set of signals with lower intensity originates from minor isomers due to *cis*-*trans* isomerization of the carbamate moieties, as was shown by observation of corresponding exchange signals in ROESY spectra.

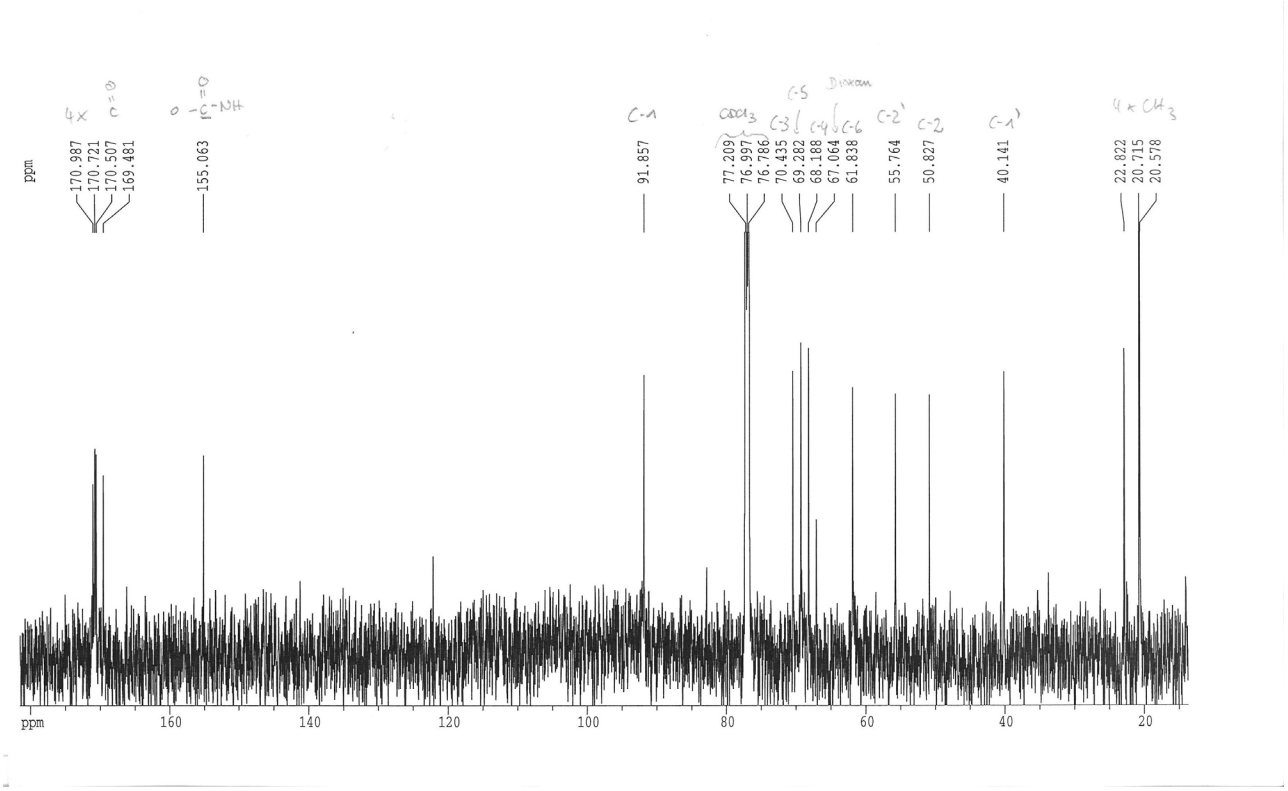

^{13}C NMR of **19** ($CDCl_3$, 150.9 MHz)

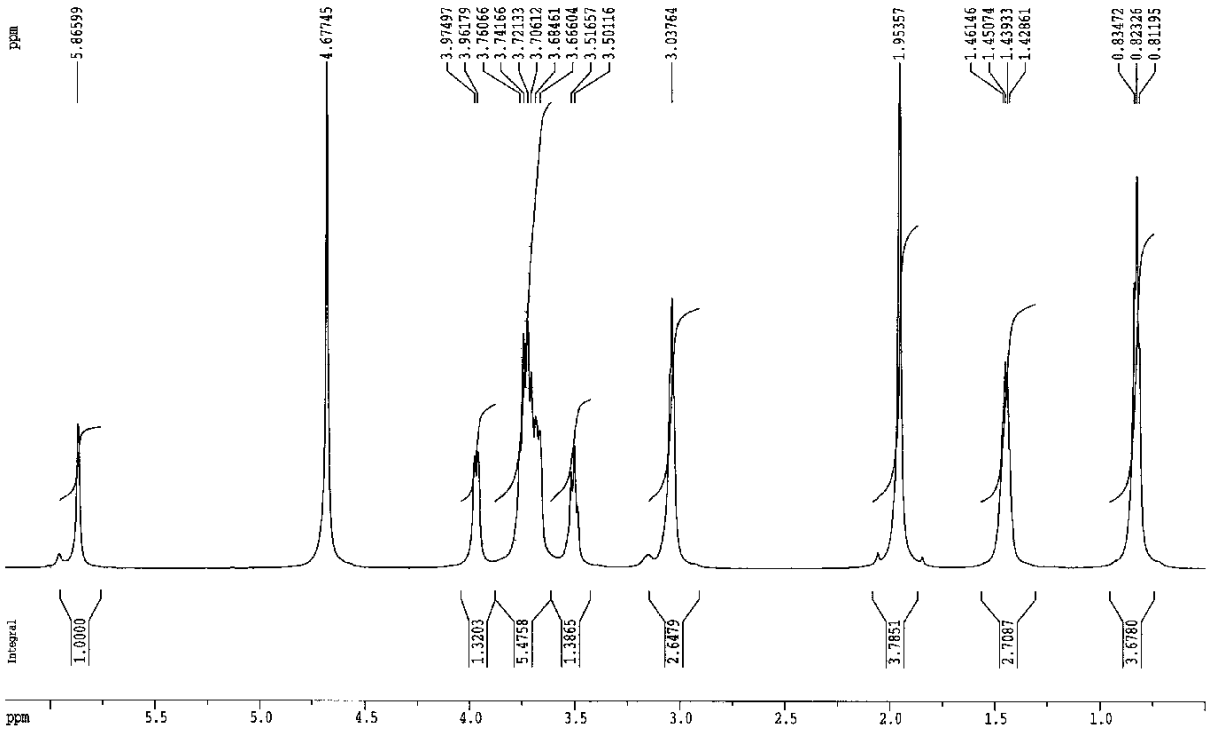

^{1}H NMR of **20** (D_2O, 600.1 MHz)

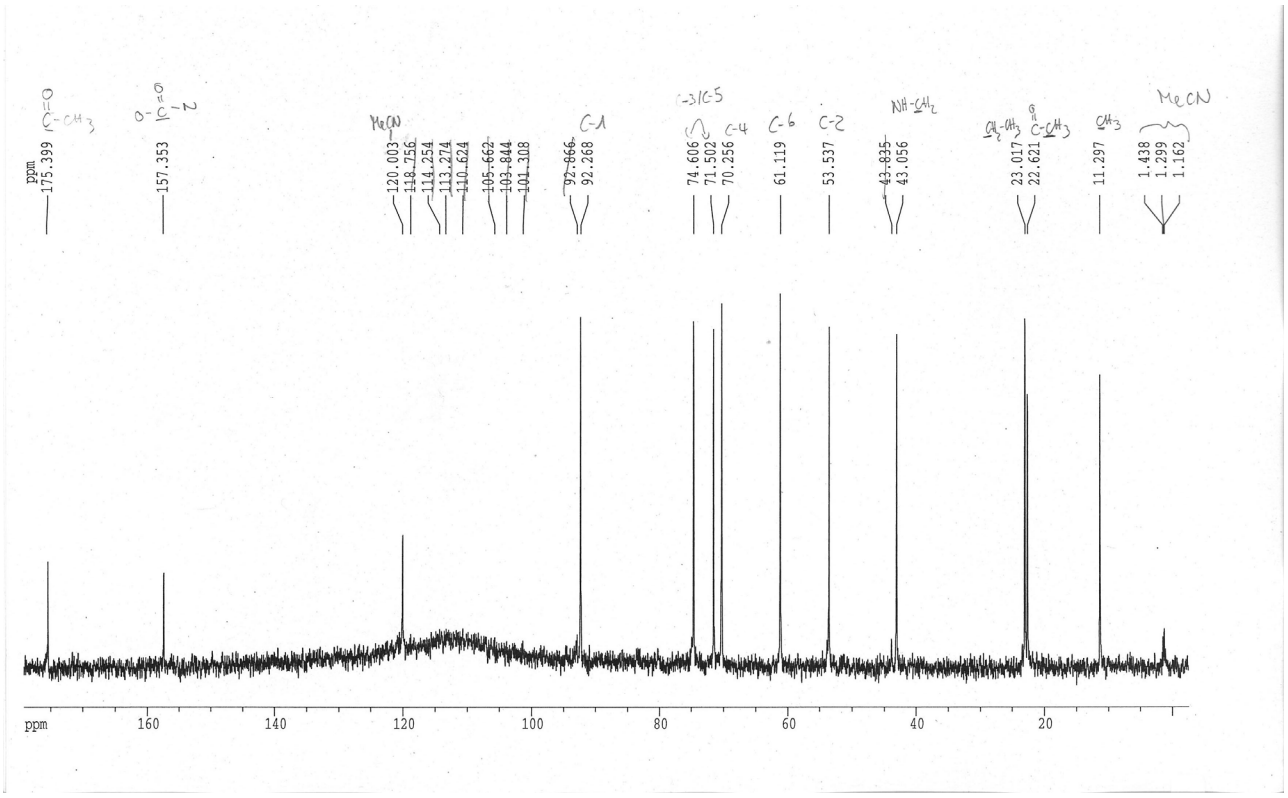

^{13}C NMR of **20** (D_2O, 150.9 MHz)

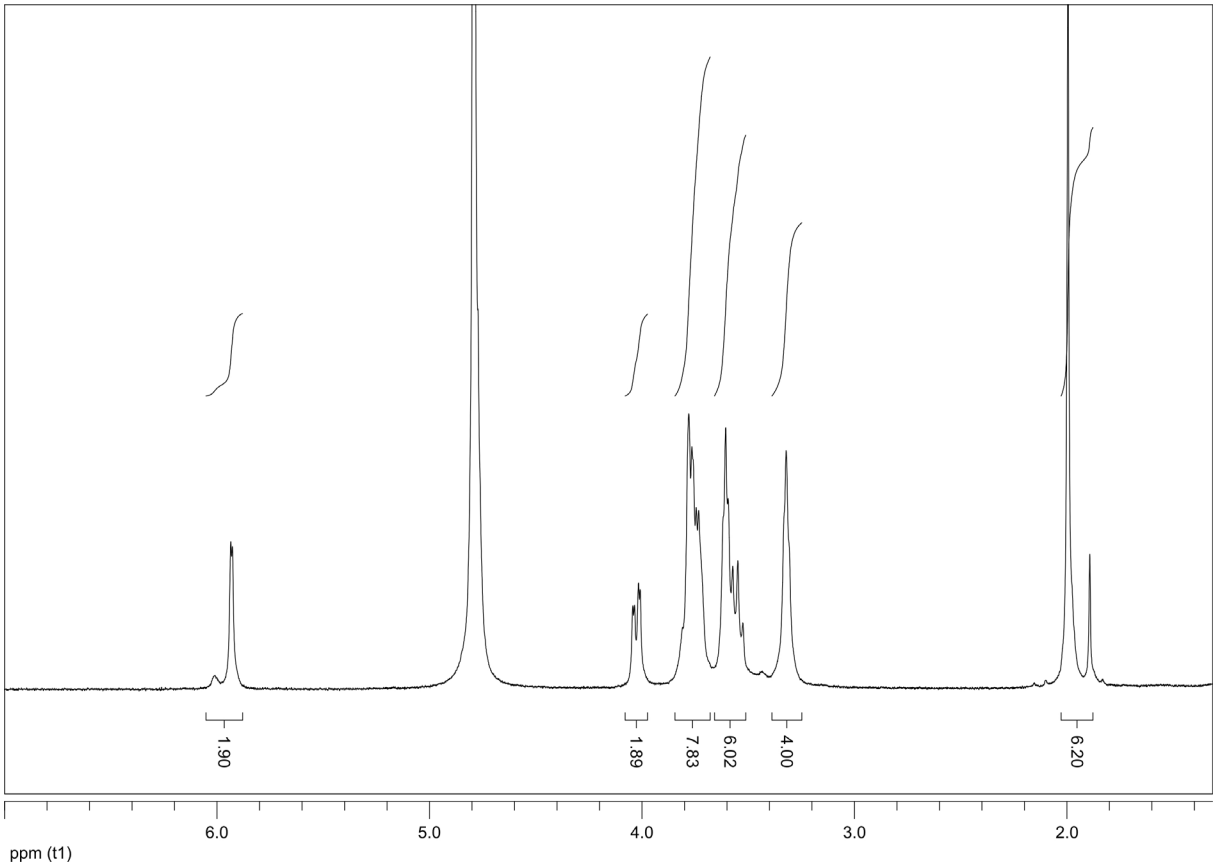

^{1}H NMR of **21** (D_2O, 400.1 MHz)

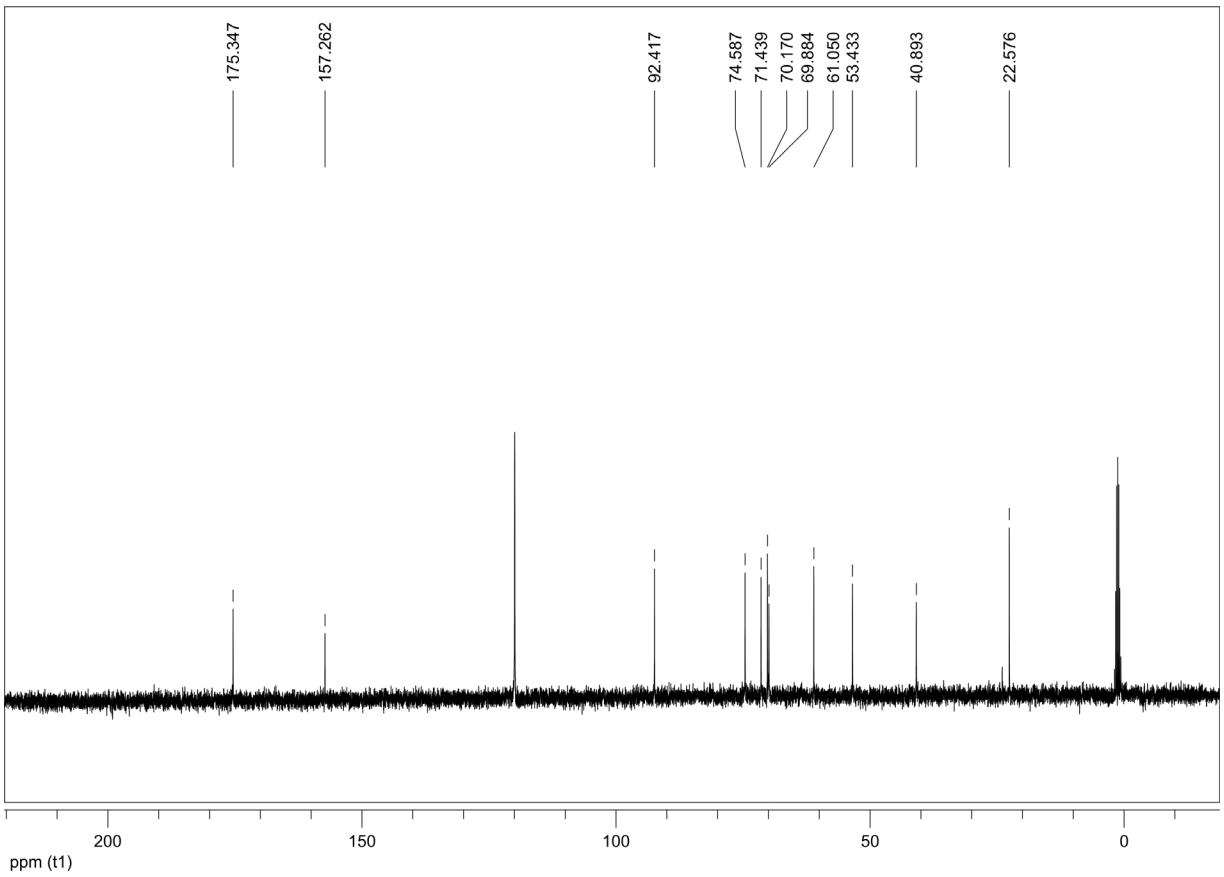

^{13}C NMR of **21** (D_2O, 100.6 MHz)

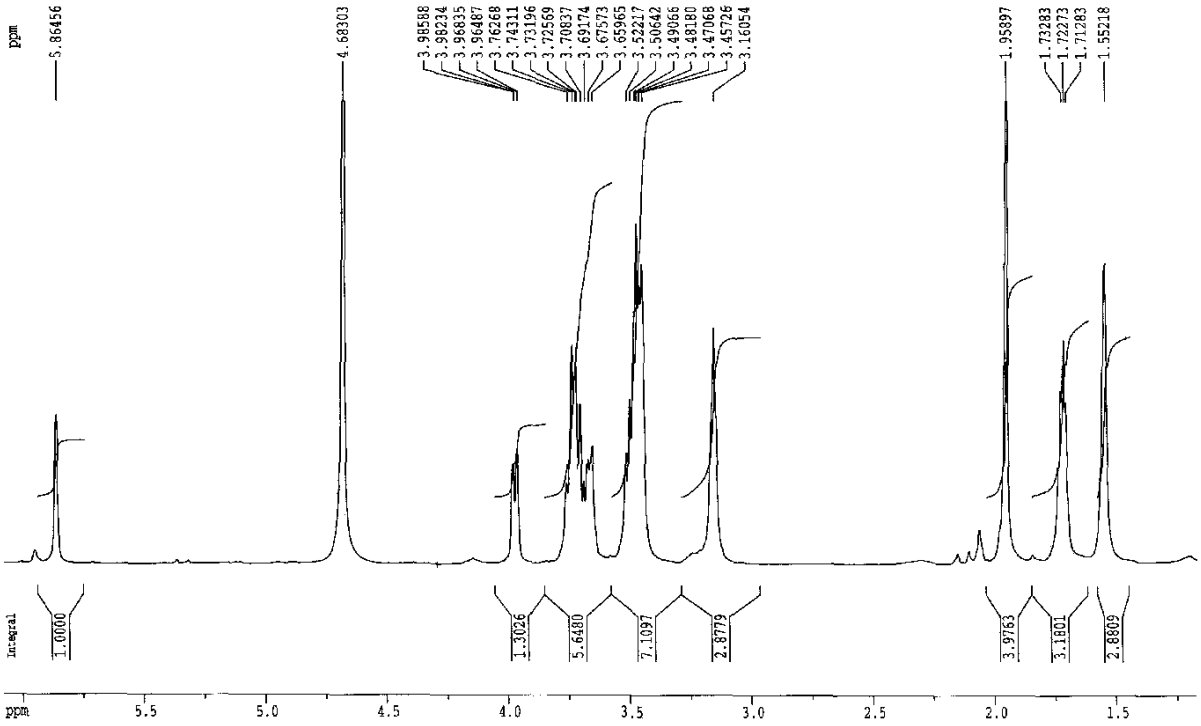

^{1}H NMR of **22** (D_2O, 600.1 MHz)

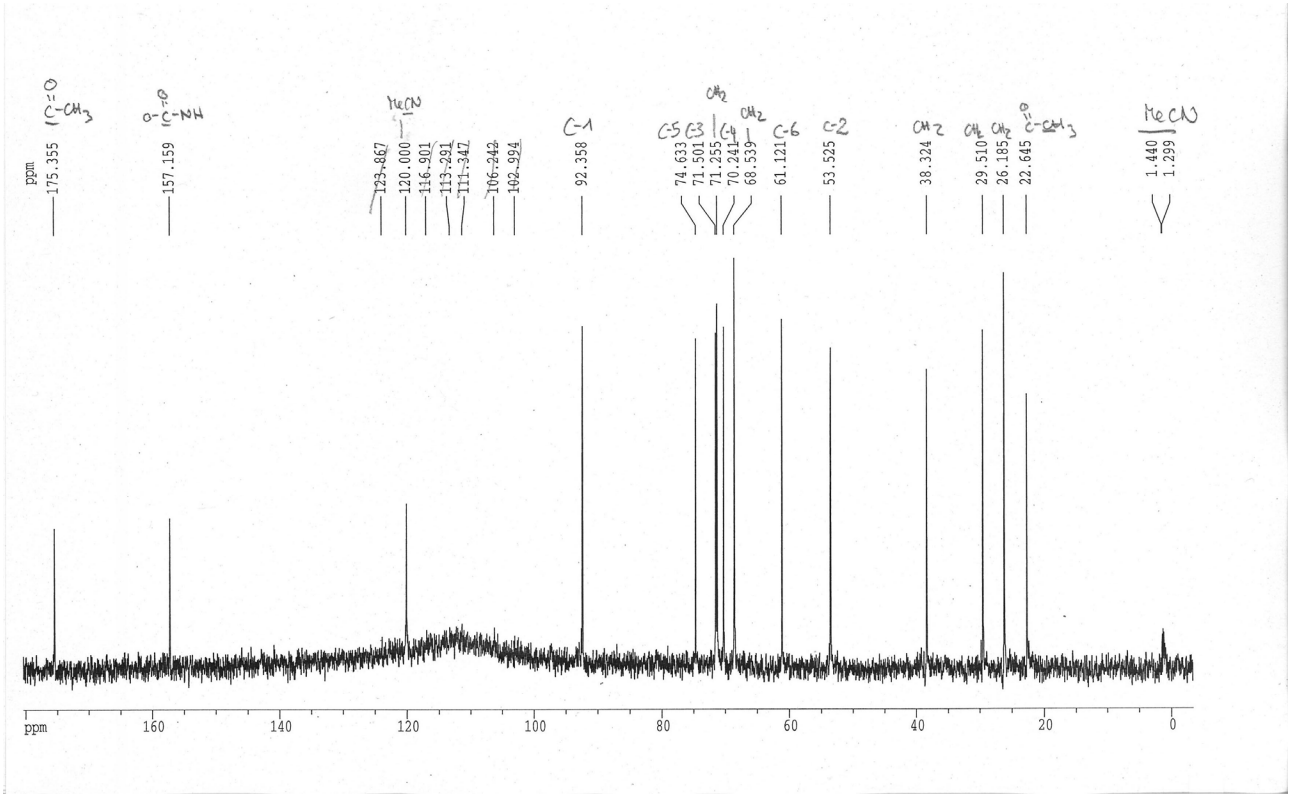

^{13}C NMR of **22** (D_2O, 150.9 MHz)

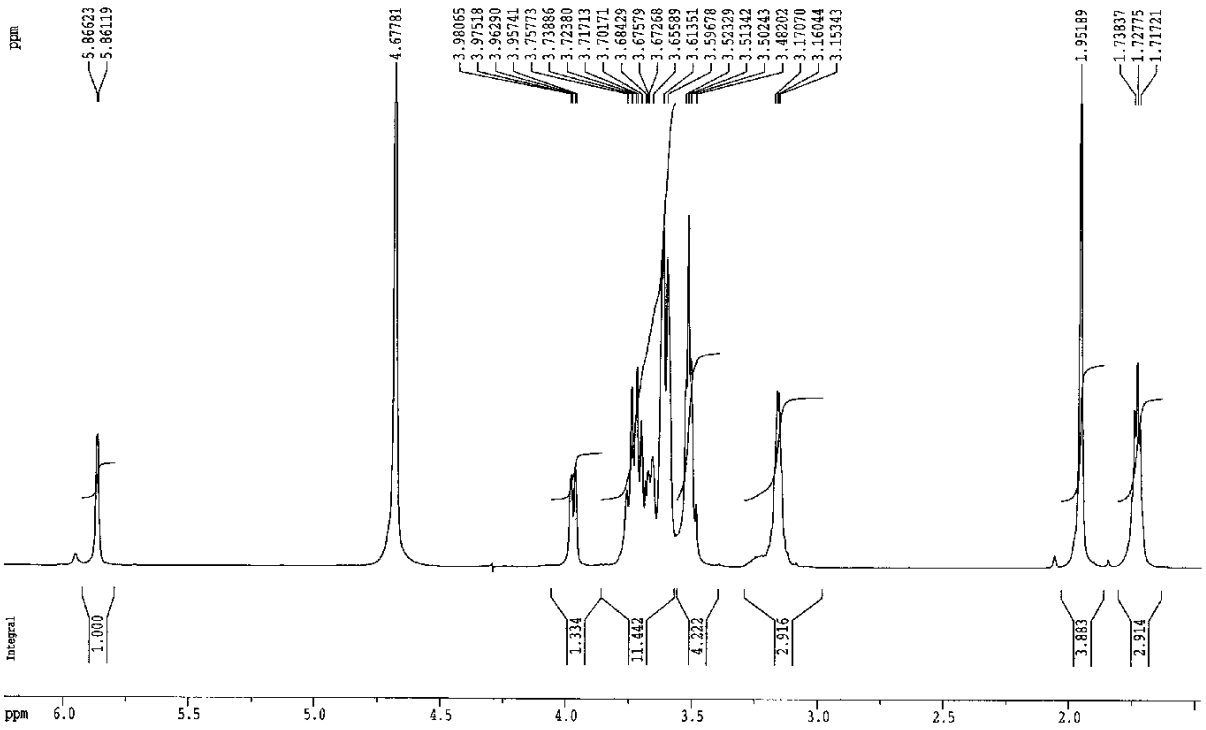

^{1}H NMR of **23** (D_2O, 600.1 MHz)

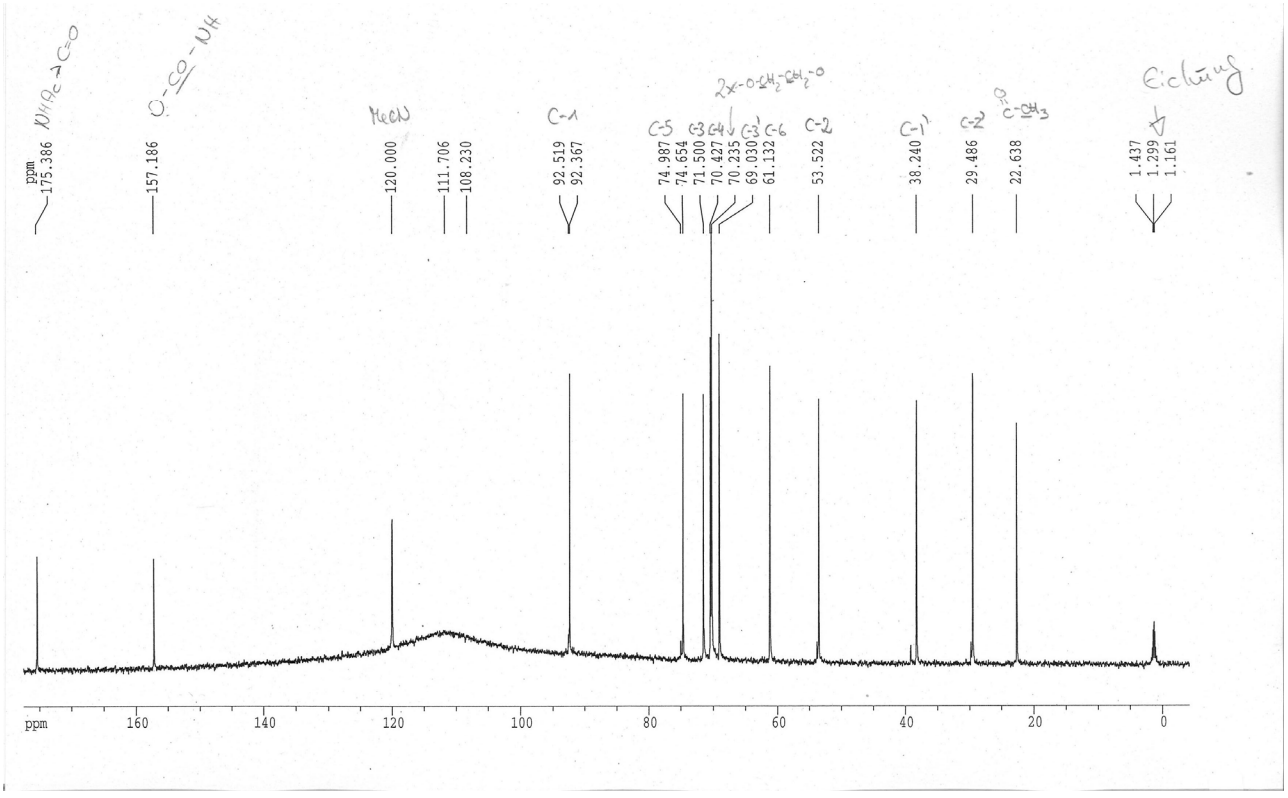

^{13}C NMR of **23** (D_2O, 150.9 MHz)

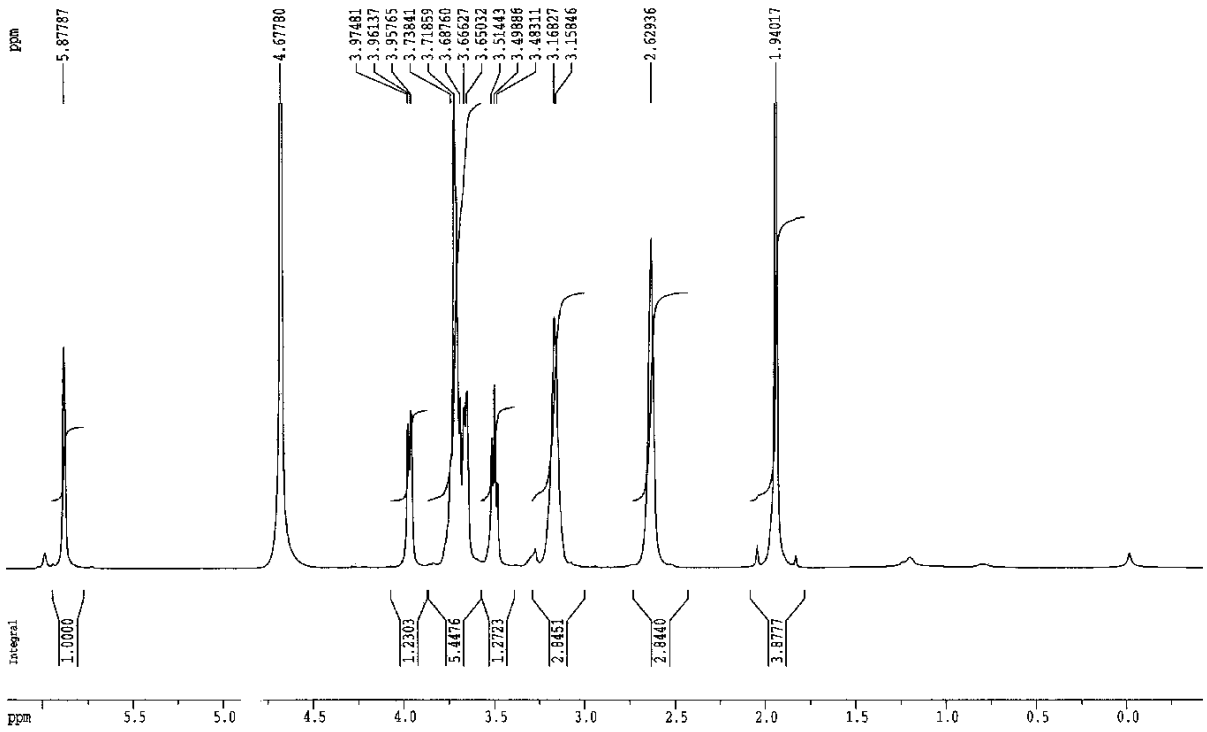

^{1}H NMR of **24** (D_2O, 600.1 MHz)

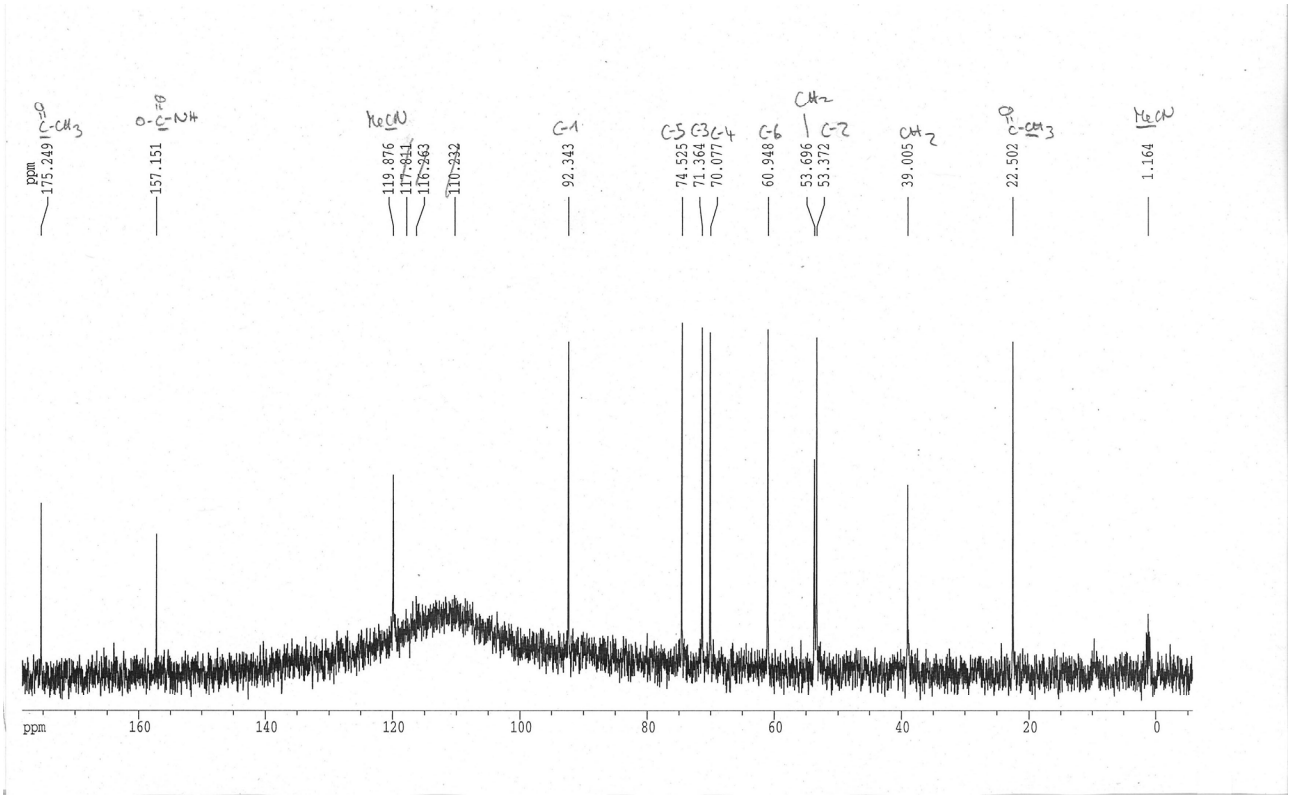

^{13}C NMR of **24** (D_2O, 150.9 MHz)

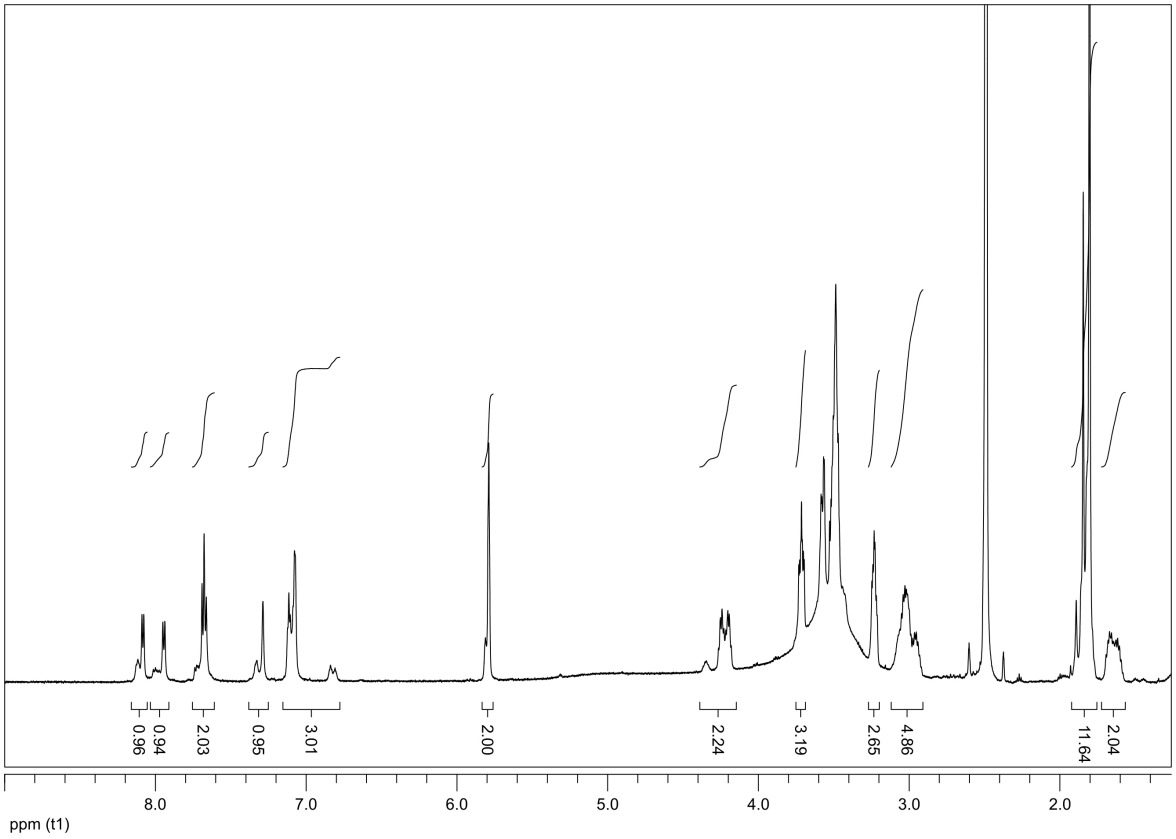

^{1}H NMR of **28** (DMSO-d_6, 600.1 MHz)*

* The set of signals with lower intensity originates from minor isomers due to *cis-trans* isomerization of the carbamate moieties, as was shown by observation of corresponding exchange signals in ROESY spectra (cf. below).

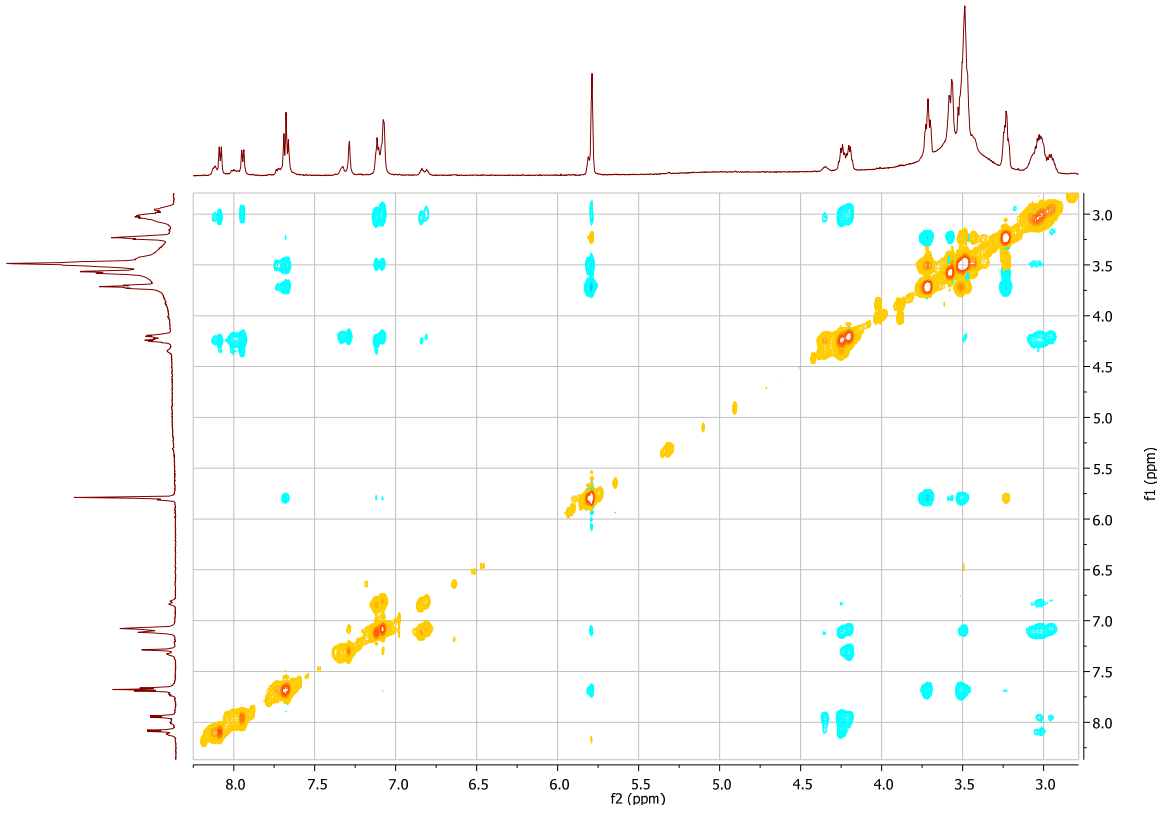

ROESY NMR of **28** (DMSO-d_6, 600.1 MHz). Orange cross peaks (with the same sign as the diagonal) indicate chemical exchange whereas cyan cross peaks originate from dipolar cross relaxation (spatial vicinity).

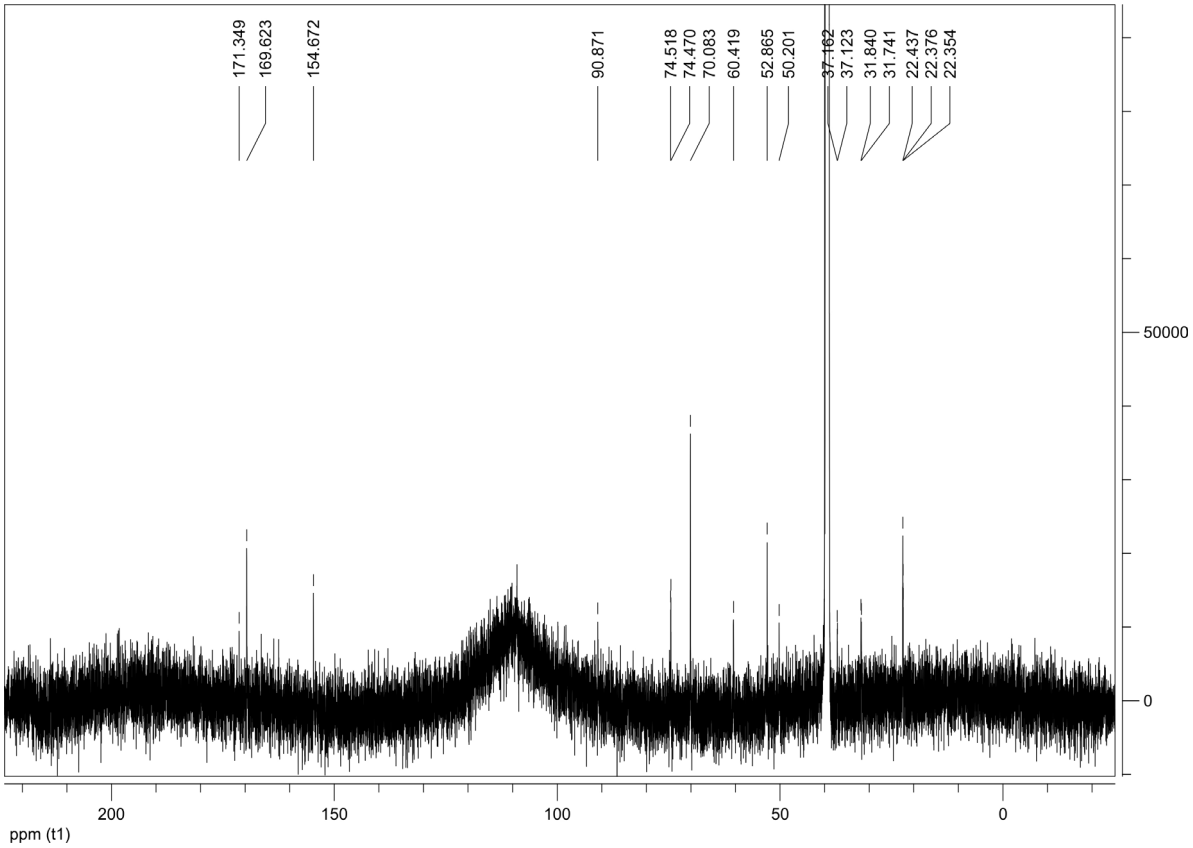

^{13}C NMR of **28** (DMSO-d_6, 150.9 MHz)